PERGAMON

International Journal of Solids and Structures 38 (2001) 4987–5005

INTERNATIONAL JOURNAL OF SOLIDS and STRUCTURES

www.elsevier.com/locate/ijsolstr

A numerical study of T-stress in dynamically loaded fracture specimens

K.R. Jayadevan [a], R. Narasimhan [b,*], T.S. Ramamurthy [a], B. Dattaguru [a]

[a] *Department of Aerospace Engineering, Indian Institute of Science, Bangalore 560 012, India*
[b] *Department of Mechanical Engineering, Indian Institute of Science, Bangalore 560 012, India*

Received 9 May 2000; in revised form 17 August 2000

Abstract

The objective of this paper is to study the evolution of T-stress in dynamically loaded fracture specimens. To this end, two-dimensional plane strain, elastodynamic finite element analyses of single edge notched (tension) specimens, and three point bend specimens subjected to time varying loads are performed. The T-stress is computed using an accurate and computationally efficient domain representation of the interaction integral. The results demonstrate that dynamically loaded specimens are subjected to a large negative T-stress during the early stages of loading as compared to that under static loading. The above phenomenon can satisfactorily explain the strong elevation in the dynamic fracture toughness at high loading rates, which has been reported in numerous experimental studies.

Keywords: Dynamic loading; Dynamic fracture toughness; T-stress; K–T locus; Finite elements

1. Introduction

The precise knowledge of the dynamic fracture behaviour of engineering materials at high loading rates is very important in the fracture analysis of large structural systems subjected to dynamic loading. Some examples of such systems are space station modules subjected to micro-meteroid impact, blast loading in an aircraft, etc. (Kanninen and O'Donoghue, 1995).

Experimental studies show that the dynamic fracture toughness of engineering materials is a function of the stress intensity rate, $\dot{K}$. It is generally observed that the dynamic fracture toughness associated with very high loading rates is significantly higher than the static fracture toughness (Ravi-Chandar and Knauss, 1984; Kalthoff, 1986; Dally and Barker, 1988; Zehnder and Rosakis, 1990). In a very recent investigation, Owen et al. (1998a) conducted dynamic fracture initiation experiments using single-edge notch (SEN)

* Corresponding author. Tel.: +91-80-309-2589; fax: +91-80-360-0648.
E-mail address: narasi@mecheng.iisc.ernet.in (R. Narasimhan).

0020-7683/01/$ - see front matter
PII: S0020-7683(00)00323-1

specimens made of 2024-T3 aluminium alloy. They used a servo-hydraulic testing machine to obtain fracture data at low loading rates ($\dot{K} < 10^4$ MPa $\sqrt{\text{m}}$/s) and also a split-Hopkinson bar set-up to gather data at high loading rates (i.e., $\dot{K} > 10^5$ MPa $\sqrt{\text{m}}$/s). Their results show that the fracture toughness is approximately the same as the quasi-static value for $\dot{K}$ less than 10^5 MPa $\sqrt{\text{m}}$/s. On the other hand, it shows a steep elevation above the quasi-static value for $\dot{K}$ greater than 10^5 MPa $\sqrt{\text{m}}$/s. Similar results were obtained by Owen et al. (1998b) and Venkert et al. (1998) for beryllium-bearing bulk metallic glasses and Ni–Cr steels, respectively.

The above phenomenon has not been satisfactorily explained through analytical studies. Kalthoff (1986) proposed the existence of an incubation time to modify the static instability fracture criterion. Ravi-Chandar and Knauss (1984) also arrived at the conclusion of a minimum time requirement for fracture initiation. In a more recent work, Liu et al. (1998) have analytically modelled the experimental configuration used by Ravi-Chandar and Knauss (1984) and obtained a transient elastodynamic solution. This solution shows a decrease in magnitude of stresses from the elastic K-field near the crack tip. Liu et al. (1998) modelled fracture initiation in terms of activating a flaw at some distance from the crack tip, when the normal stress across the defect attains a critical value. The observed increase in fracture toughness was attributed to the finite time required to achieve a critical stress state ahead of the crack tip over a characteristic length. The work of Liu et al. (1998) is an important contribution since it provides for the first time an explanation for the observed increase in fracture toughness of engineering materials at high loading rates based on an analytical study of inertial effects in the near-tip fields. It provides impetus for undertaking a systematic investigation of the effects of loading rate, crack length and specimen geometry on the stress field near the crack tip with the view of rationalizing the experimentally observed dynamic fracture behaviour.

The traditional fracture mechanics approach assumes that a single parameter such as K in linear elastic materials, or J in elastic–plastic materials, fully characterizes the crack tip field. However, for certain geometries and loading configurations, the validity of the single parameter characterization has been found to be inadequate (see, e.g., Al-Ani and Hancock, 1991; O'Dowd and Shih, 1992). In this context, the importance of the elastic T-stress, which is the second term in the series solution for the stress field near the crack tip in an elastic solid (Williams, 1957), is well studied in the literature for quasi-static loading. In an early investigation, Larsson and Carlsson (1973) showed that the elastic T-stress can have a significant effect on the size and shape of the plastic zone around the crack tip under small scale yielding conditions.

Betegon and Hancock (1991) showed that the crack tip fields in fracture configurations can be adequately described by the stress intensity factor and T-stress. O'Dowd and Shih (1992) argued that the T-stress is a parameter based on elastic analysis and hence cannot be used to characterize crack tip fields under large scale plasticity. Hence, they proposed the J–Q theory, where Q is a stress triaxiality parameter. A negative Q indicates loss of stress triaxiality or *constraint* near the crack tip. However, for small to intermediate scale yielding conditions, the J–T theory is fully equivalent to the J–Q approach (see O'Dowd and Shih, 1992).

O'Dowd and Shih (1994) predicted the cleavage fracture toughness of two steels corresponding to different Q values using a critical stress criterion. They found that the predicted cleavage fracture toughness increases strongly with negative Q-stress and also agrees well with the experimental data of Kirk et al. (1993) and Sumpter and Forbes (1992). Betegon et al. (1996) made similar predictions for the effect of T-stress on the cleavage fracture toughness of a high strength low carbon steel. They also concluded that the fracture toughness increases strongly with negative T-stress and matches well with experimental data. Roy and Narasimhan (1999a) have studied the effect of T-stress on the ductile fracture processes of microvoid growth and coalescence. They found that a large negative T-stress can significantly retard the above processes under mode-I loading and, hence, can elevate the fracture toughness of ductile alloys. This was confirmed from an experimental investigation by Roy et al. (1999) using a ductile 2014-O aluminium alloy.

By contrast, very little research work has been devoted to understand the role of T-stress (or, equivalently, the Q-stress for ductile solids) on fracture processes under dynamic loading. A first step in this direction was taken by Koppenhoefer and Dodds (1996) who studied the evolution of Q-stress in impact-loaded pre-cracked ductile Charpy specimens. Their results indicate a negative Q-stress throughout the loading history. In a more recent study, Basu and Narasimhan (2000a) carried out a systematic investigation of loading rate and crack length on Q-stress in dynamically loaded fracture specimens. They found that a specimen which shows no constraint loss under static loading, can exhibit strong negative Q-stress when loaded dynamically. This satisfactorily explains the retardation in the ductile fracture processes of micro-void growth and coalescence at high loading rates reported by Basu and Narasimhan (1996, 1999, 2000b). It also helps in understanding the enhancement in fracture toughness of ductile materials at very high loading rates (Owen et al., 1998a,b; Venkert et al., 1998). Since the Q-stress and T-stress are related under small scale yielding conditions and static loading (see, O'Dowd and Shih, 1992), it may be expected based on the conclusions of Liu et al. (1998) and Basu and Narasimhan (2000a) that the T-stress may be dramatically affected under dynamic loading in typical fracture specimens. Hence, a careful investigation of the evolution of T-stress in dynamically loaded linear elastic fracture specimens is warranted.

Thus, the main objective of the present study is to examine the dependence of T-stress on specimen geometry, crack length and loading rate in dynamically loaded specimens. Following the approach of Betegon and Hancock (1991) in quasi-static fracture mechanics, a two-parameter fracture model based on K and T is proposed, which can explain well the enhancement in fracture toughness of engineering materials at high loading rates. To this end, two-dimensional (2-D) plane strain transient finite element analyses of a SEN specimen subjected to a tensile stress pulse (SEN(T)), and an impact loaded three-point bend specimen (TPB) are conducted. Several crack length to width ratios a/W ranging from 0.2 to 0.7 are considered. The loading rate $\dot{K}$ is varied from a moderate value of 10^5 to a very high value of about 10^7 MPa $\sqrt{\text{m}}$/s. The energy release rate $\mathscr{G}$ is evaluated using the domain integral method (Nakamura et al., 1986). The evolution of elastodynamic T-stress is computed for each case using the interaction integral (Sladek et al., 1997). The results show that the T-stress has a very strong negative value during early stages of dynamic loading albeit it may be positive or small in magnitude under static loading.

2. Numerical analysis

2.1. Modelling aspects

Two specimen geometries are analysed in this work. The first specimen considered is a single edge notched plate subjected to tensile loading (SEN(T)) as shown in Fig. 1(a). The length $2L$ and width W of the specimen are taken as 160 and 40 mm, respectively. The ratios of crack length a to the width W considered in the analyses are $a/W = 0.7$, 0.5 and 0.2. The boundary conditions applied on the specimen are as shown schematically in Fig. 1(a). Since the load versus time curves obtained from impact testing of fracture specimens generally exhibit a highly non-linear variation (see, e.g., Zehnder et al., 1990) the applied load $P(t)$ is chosen as a function of time t in the form $P(t) = \alpha t + \gamma t^2$. By varying the constants α and γ, a range of stress intensity rates, $\dot{K}$, is achieved at the crack tip. Further, as shown in Fig. 1(a), the load P is uniformly distributed on the edge $X_2 = +L$.

A typical finite element mesh used to represent the SEN(T) specimen with $a/W = 0.7$ is shown in Fig. 2(a). In this case, the complete specimen needs to be represented because wave propagation effects render this geometry unsymmetric with respect to the crack plane. This mesh comprises of 1932 four noded (2-D plane strain) quadrilateral elements and 2024 degrees of freedom. The details of the refined mesh near the

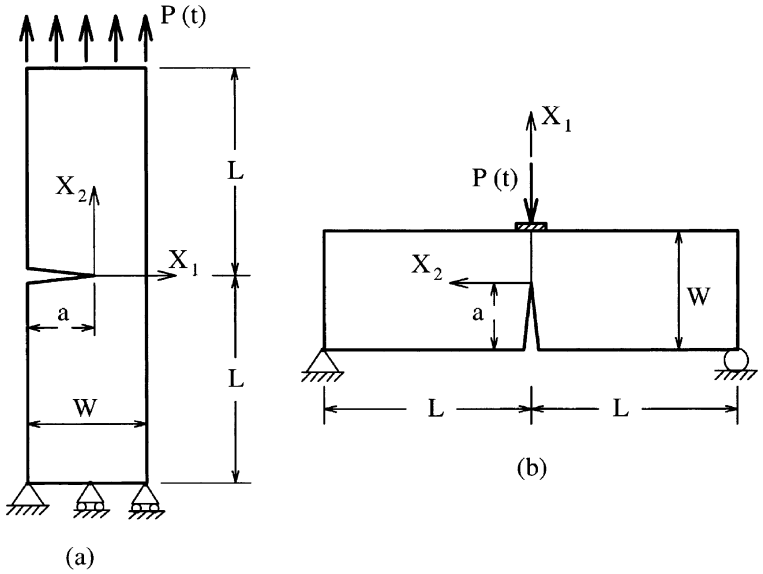

Fig. 1. Schematic of (a) SEN(T) and (b) TPB specimen.

tip is shown in Fig. 2(b). As can be seen from this figure, a focussed mesh having concentric rings of elements surrounding the crack tip is employed. The smallest element size near the crack tip in this mesh is about 0.116 mm which is less than $0.01\,(W-a)$. The above focussed near-tip mesh merges smoothly with an outer region in which the element size gradually increases towards the boundaries. Similar meshes with good refinement near the crack tip were used for analyses with other a/W ratios. A mesh convergence study was performed by conducting a few analyses with a mesh having more elements near the crack tip than that shown in Fig. 2(b). It was found from these analyses that the evolution histories of important quantities like J-integral and T-stress are well represented by the meshes employed in this work. A mesh sensitivity study was also carried out by comparing the results obtained using a mesh generated by an automatic mesh generation programme and a structured mesh with focussed elements near the tip as shown in Fig. 2. The results obtained from these different meshes for the J-integral and T-stress were within 1% to 2% of each other. However, the domain independence (see also Section 2.2) was better for the structured mesh and, hence, it is selected for this study.

The second fracture geometry (see Fig. 1(b)) modelled in this work, is a TPB specimen subjected to impact-type loading, which is widely used in dynamic fracture testing (Zehnder and Rosakis, 1990; Zehnder et al., 1990). The length and width of the TPB specimen are chosen identical to that of the SEN(T) specimen. The boundary conditions applied on the specimen are also shown schematically in Fig. 1(b). The a/W ratios considered in the analysis of the TPB specimen are 0.7, 0.5 and 0.2. Since the SEN(T) and TPB specimens have the same geometry, meshes similar to Fig. 2 are employed in analyzing the TPB specimen also, except that due to symmetry, only half the specimen is modelled. Further, a fine mesh is used near the loading point and the applied load is distributed as a uniform traction over a small distance of about 2 mm in order to reduce numerical errors. The applied load $P(t)$ is chosen to have the same functional variation with respect to time as the SEN(T) specimen.

In addition to the dynamic analyses, static analysis of each specimen is conducted in order to compute its biaxiality parameter ($\beta = T\sqrt{\pi a}/K$, where a is the crack length) under static loading. The material properties employed in all the analyses are $E = 200$ GPa, $v = 0.3$, and ρ(density) $= 7800$ kg/m^3. In the dynamic

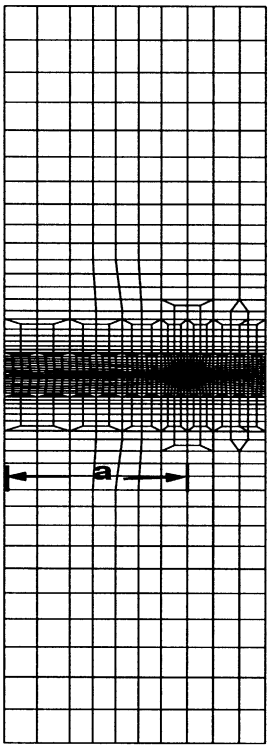

(a)

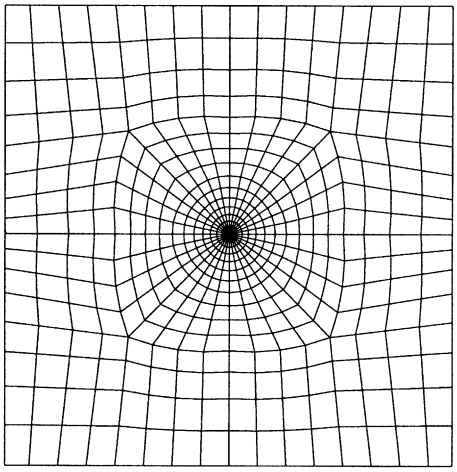

(b)

Fig. 2. (a) Finite element model of the SEN(T) specimen. Crack length is marked as *a*. (b) Enlarged view of mesh used near the crack tip.

analyses, the equations of motion are integrated using the explicit central difference scheme (Zienkiewicz and Taylor, 1989). Since this time integration scheme is only conditionally stable, the time step size Δt chosen as less than the critical time step $\Delta t_{cr} = 2/\omega_{max}$, where ω_{max} is the maximum eigenvalue of the finite element system.

2.2. Computation of energy release rate and T-stress

The expression for the energy release rate corresponding to a dynamically loaded stationary crack tip in an elastic solid is given by (Nakamura et al., 1986):

$$\mathscr{G} = \lim_{\Gamma \to 0} \int_{\Gamma} \left[(W + L) n_1 - \sigma_{ij} n_j \frac{\partial u_i}{\partial x_1} \right] \mathrm{d}\Gamma. \tag{1}$$

Here, σ_{ij} and u_i are the cartesian components of stress and displacement, and n_i are the components of unit outward normal vector to Γ (see Fig. 3(a)), which is a vanishingly small contour surrounding the crack tip. The quantities W and L are the elastic strain energy and kinetic energy densities, respectively. A domain integral version of Eq. (1) proposed by Nakamura et al. (1986), is employed to compute $\mathscr{G}$ from the finite element results. Several rectangular and circular domains (with outer dimension ranging from $0.3b$ to $0.7b$, where b is the minimum of a and $(W - a)$ are employed to evaluate $\mathscr{G}$. It is found that the maximum percentage variation in $\mathscr{G}$ obtained from different domains is within 0.5% at any instant of time. The stress intensity factor K is obtained from the average value of $\mathscr{G}$ determined from the different domains using the relation $\mathscr{G} = K^2(1 - \nu^2)/E$ (assuming plane strain). Further, an average loading rate $\dot{K}$ is computed from the stress intensity factor history obtained for each analysis.

In order to evaluate the elastodynamic T-stress accurately, the interaction integral is employed. This is given by,

$$M = \mathscr{G}^{A+B} - \mathscr{G}^{A} - \mathscr{G}^{B}, \tag{2}$$

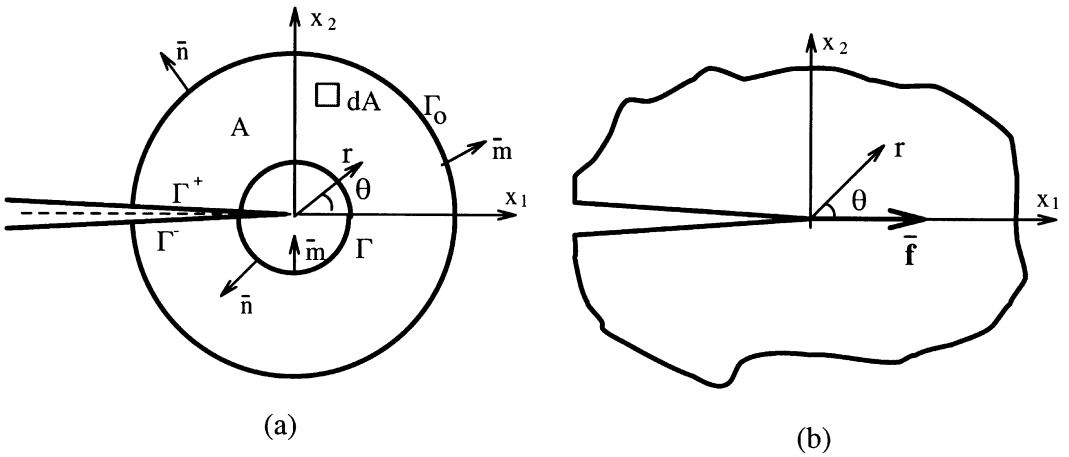

Fig. 3. Schematic showing an annular area A enclosed between a vanishingly small contour Γ, arbitrary outer contour Γ_o surrounding the crack tip, and the crack faces Γ^+ and Γ^-. (b) Schematic of semi-infinite crack with point load $\tilde{f}$ applied at the tip parallel to x_1 direction.

where, $\mathscr{G}^A$ and $\mathscr{G}^B$ are the energy release rates (see Eq. (1)) corresponding to the original dynamic field A and an auxiliary static field B, respectively, and $\mathscr{G}^{(A+B)}$ is that pertaining to the field combining A and B. Using Eq. (1), the final expression for the interaction integral can be shown to be:

$$M = \lim_{\Gamma \to 0} \int_{\Gamma} \left[\sigma_{ij}^A \varepsilon_{ij}^B n_1 - \sigma_{ij}^A n_j u_{i,1}^B - \sigma_{ij}^B n_j u_{i,1}^A \right] \mathrm{d}\Gamma. \tag{3}$$

Kfouri (1986) and Sladek et al. (1997) selected the auxiliary problem as that of a semi-infinite crack subjected to a point load $\tilde{f}$ at the crack tip in the direction of crack line (see Fig. 3(b)). On using this auxiliary field in Eq. (3), a simple relation between the interaction integral and the T-stress pertaining to the original field can be derived for the plane strain case as,

$$M = \frac{(1-\nu^2)}{E} T \tilde{f}. \tag{4}$$

The expressions for the auxiliary fields and the detailed derivation of the above relation for a dynamically loaded crack tip are given by Sladek et al. (1997).

In this work, the interaction integral given by Eq. (3) is converted to an area integral following the approach suggested by Nakamura et al. (1986) in order to facilitate its easy and accurate computation from the finite element results. The expression for the domain integral version of Eq. (3) is given by,

$$M = \lim_{\Gamma \to 0} \int_{A} \left[\left(\sigma_{ij}^A \frac{\partial u_i^B}{\partial x_1} + \sigma_{ij}^B \frac{\partial u_i^A}{\partial x_1} \right) \frac{\partial q}{\partial x_j} - \sigma_{ij}^A \varepsilon_{ij}^B \frac{\partial q}{\partial x_1} + \rho \ddot{u}_i^A u_{i,1}^B q \right] \mathrm{d}A. \tag{5}$$

In this equation, q is a weighting function which has a value of unity on the vanishingly small inner contour Γ surrounding the crack tip and zero on an arbitrary outer contour Γ_o (see Fig. 3(a)). In the annular area A enclosed between Γ, Γ_o and the upper lower crack faces Γ^+ and Γ^- (Fig. 3(a)), the function $q(x_1, x_2)$ is assumed to be smooth but is otherwise arbitrary. The last term in Eq. (5) arises from inertia effects and can be neglected for quasi-static loading.

Before pursuing the actual analyses, the computation of T-stress using the method presented above was extensively tested by studying a few benchmark problems in elastostatic as well as in elastodynamic fracture. A crack of length $2a$ in an infinite plate subjected to a quasi-static, far-field, uniform tension normal to the crack plane (Griffith's problem) was considered and the computed T-stress deviated from the exact value by about 0.05%. In the elastodynamic case, a semi-infinite crack in a strip subjected to a tensile stress wave (Freund, 1990) normal to the crack plane was chosen as the benchmark problem. Again, an excellent agreement between the computed T-stress history and the analytical result given by Freund (1990) was noted.

The interaction integral (Eq. (5)) is computed from the results of the finite element analyses of the SEN(T) and TPB specimens using several rectangular and circular domains with size ranging from $0.3b$ to $0.7b$, where b is the minimum of the crack length and uncracked ligament length. The maximum percentage variation in T-stress values computed from the different domains was found to be less than 1% at any instant of time in all the analyses.

3. Results and discussion

In this section, the results obtained from the finite element analyses are presented. In Table 1, the biaxiality parameter β, computed for SEN(T) and TPB specimens with different a/W ratios under static

Table 1
Biaxiality parameters corresponding to different a/W ratios for the SEN(T) and TPB specimens

Specimen	a/W ratio		
	0.2	0.5	0.7
SEN(T)	−0.448	−0.158	+0.203
TPB	−0.256	+0.117	+0.432

Biaxiality Parameter, $\beta = T\sqrt{\pi a}/K$.

loading are tabulated. The results presented in Table 1 compare very well with the corresponding biaxiality ratios given by Kfouri (1986).

3.1. SEN(T) specimen

Results obtained from the dynamic analyses of SEN(T) specimen are presented in Figs. 4–8. In Figs. 4 and 5, typical time histories of the stress intensity factor computed for the SEN(T) specimen with a/W ratio of 0.7 and 0.2, respectively, are shown. The coefficients α and γ of the loading function $P(t)$, which are given

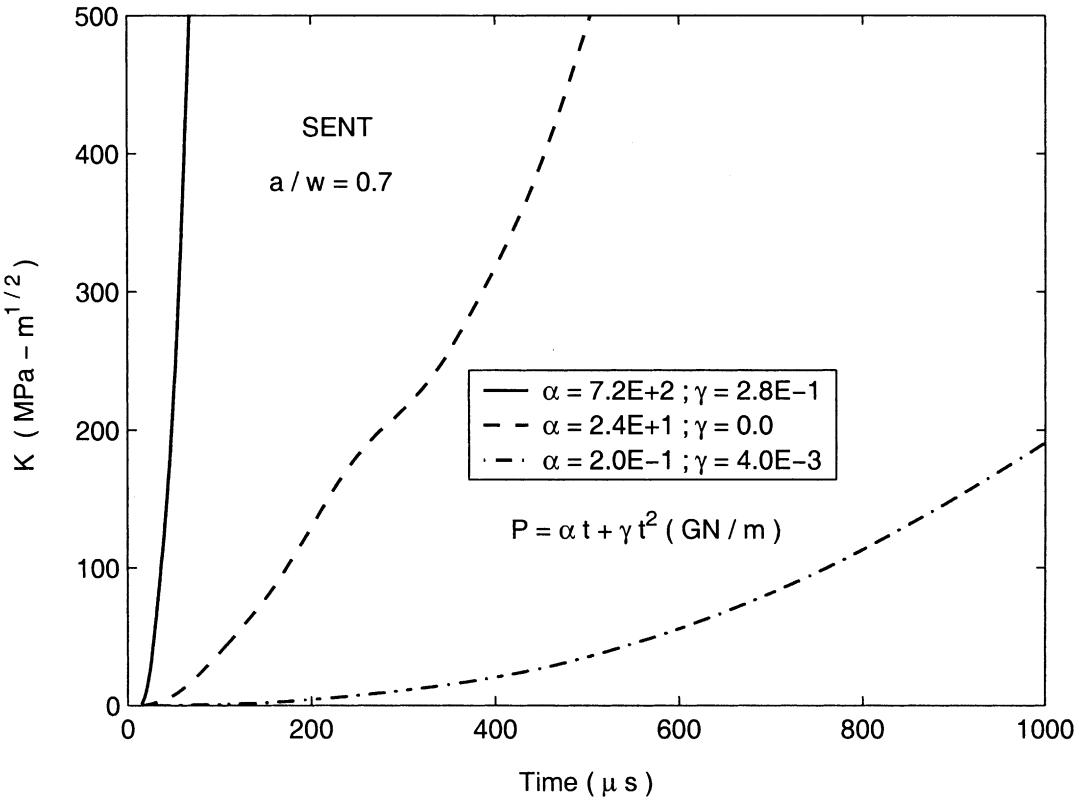

Fig. 4. Typical time histories of stress intensity factor obtained for SEN(T) specimen with $a/W = 0.7$.

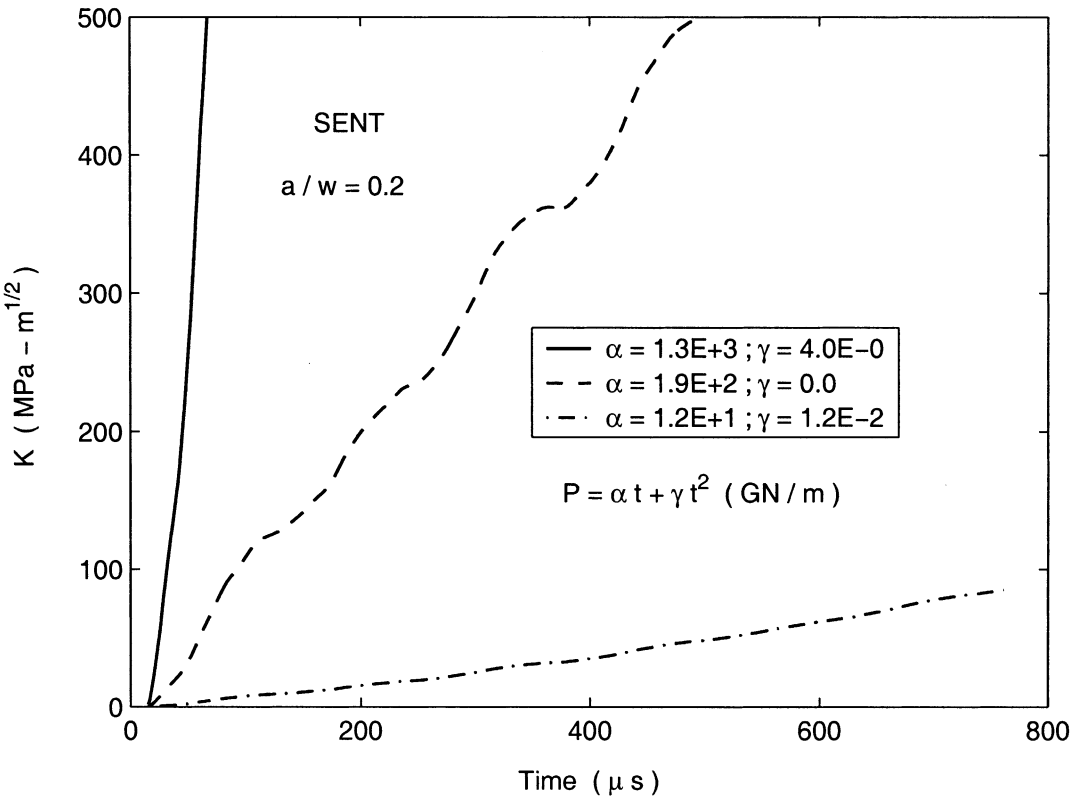

Fig. 5. Typical time histories of stress intensity factor obtained for SEN(T) specimen with $a/W = 0.2$.

as legend in these figures are chosen by trial and error so that stress intensity rates $\dot{K}$ vary in the range of 10^5–10^7 MPa$\sqrt{\text{m}}$/s. A comparison of Figs. 4 and 5 shows that, a much higher load function $P(t)$ must be applied for the shallow cracked specimen than for the deep cracked specimen, in order to obtain similar time histories of stress intensity factor.

In Figs. 6–8, the evolution histories of the biaxiality parameter with the dynamic stress intensity factor are displayed for SEN(T) specimen with $a/W = 0.7$, 0.5 and 0.2, respectively. Results are presented pertaining to same three stress intensity rates $\dot{K}$ in each figure to facilitate direct comparison. Here, the average stress intensity rates $\dot{K}$ are calculated from time histories of stress intensity factor like those shown in Figs. 4 and 5. For comparison, the quasi-static biaxiality parameter obtained for each SEN(T) specimen is marked on the ordinate axis in the respective figures. The first observation that can be made from these figures is that unlike the static case, where β is independent of load and has a fixed value for a given specimen geometry and crack length, the biaxiality parameter under dynamic loading varies strongly with the stress intensity factor. It can be seen from Fig. 6 that for the deeply cracked specimen, β under dynamic loading has a large negative value at early stages of loading (i.e., when the magnitude of the stress intensity factor is small), even though the static biaxiality parameter has a small positive value. This behaviour is more pronounced at very high loading rates. Thus, for example, corresponding to a value of $K = 20$ MPa$\sqrt{\text{m}}$, the value of β in Fig. 6 is -1.36, -0.72 and -0.04 for $\dot{K} = 7.5 \times 10^6$, 1×10^6 and 2×10^5 MPa$\sqrt{\text{m}}$/s, respectively, whereas for the static case $\beta = +0.203$ (see Table 1). This clearly implies that the above

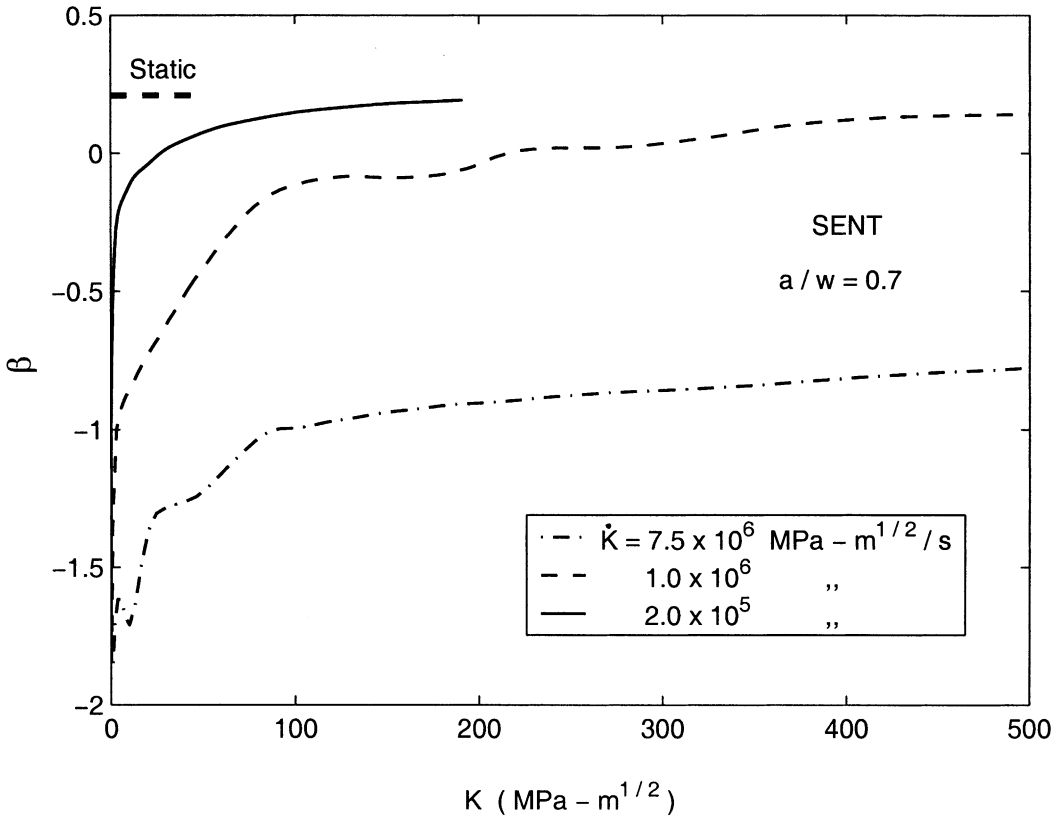

Fig. 6. Evolution histories of biaxiality parameter with stress intensity factor corresponding to different $\dot{K}$ for SEN(T) specimen with $a/W = 0.7$.

behaviour is caused by inertial effects and corroborates with the large negative Q-stress reported by Basu and Narasimhan (2000a) for dynamically loaded ductile SEN(T) specimens. As the magnitude of stress intensity factor increases (i.e., at later stages of loading), the biaxiality parameter gradually approaches the static limit. Thus, it is found that for the case $a/W = 0.7$, the biaxiality parameter computed from the dynamic analyses corresponding to $\dot{K} = 2 \times 10^5$ and 1×10^6 MPa $\sqrt{\text{m}}$/s is within 5% of the static limit for K greater than 190 and 635 MPa $\sqrt{\text{m}}$, respectively. Although, the curve corresponding to $\dot{K} = 7.5 \times 10^6$ MPa $\sqrt{\text{m}}$/s in Fig. 6 is well below the static limit at $K = 500$ MPa $\sqrt{\text{m}}$, it does indeed tend to the static limit at much higher values of K.

The evolution of β with stress intensity factor for $a/W = 0.5$ and 0.2 for different loading rates $\dot{K}$ shown in Figs. 7 and 8 are qualitatively similar to those discussed above for $a/W = 0.7$. However, it can be seen by comparing Figs. 6–8 that as the ratio of crack length to width (a/W) decreases, the biaxiality parameter approaches the quasi-static value at lower levels of K for the same $\dot{K}$. Thus, considering $\dot{K} = 1 \times 10^6$ MPa $\sqrt{\text{m}}$/s, it is found that β is within 5% of the static limit for K greater than 635, 346 and 92 MPa $\sqrt{\text{m}}$ corresponding to $a/W = 0.7$, 0.5 and 0.2, respectively. Another interesting observation that can be made from these figures is that while β becomes more negative under static loading as the normalized crack length decreases (see also Table 1), the reverse trend applies under high rates of loading. Thus, considering a stress intensity rate of $\dot{K} = 7.5 \times 10^6$ MPa $\sqrt{\text{m}}$/s, $\beta = -0.99$, -0.64 and -0.49 at $K = 100$ MPa $\sqrt{\text{m}}$ for

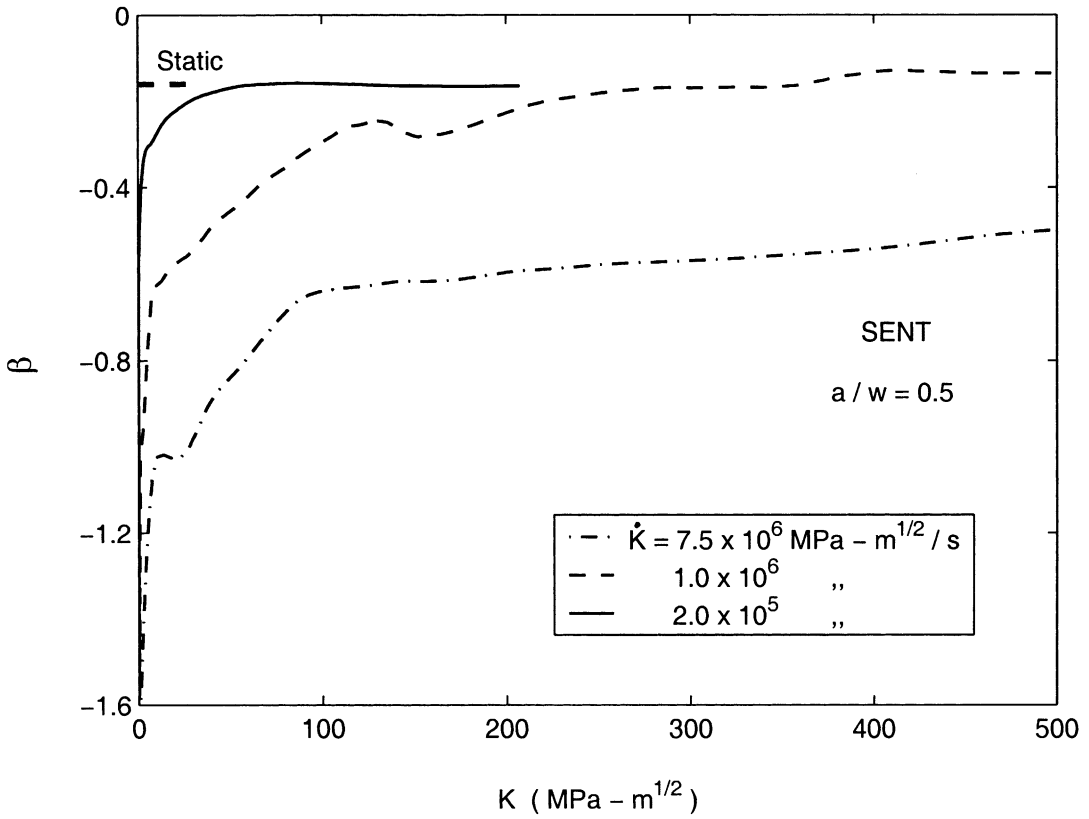

Fig. 7. Evolution histories of biaxiality parameter with stress intensity factor corresponding to different $\dot{K}$ for SEN(T) specimen with $a/W = 0.5$.

$a/W = 0.7$, 0.5 and 0.2, respectively. This implies that loss of crack tip constraint in a shallow cracked ductile SEN(T) specimen would be less as compared to a deep cracked specimen during the initial stages of dynamic loading. This is contrary to the known behaviour of these specimens under static loading (see Al-Ani and Hancock, 1991). The above trends may be attributed to difference in inertia effects experienced by the crack tip region in specimens with various crack lengths. Indeed, it was found from the numerical results that, in shallow cracked specimens the kinetic energy is comparable to the strain energy only during the initial stages of the loading, whereas in deep cracked specimen the kinetic energy continues to dominate over the strain energy for a longer time.

3.2. Three-point bend specimen

In Fig. 9, typical time histories of stress intensity factor obtained for the TPB specimen with $a/W = 0.5$ are shown. As in the case of the SEN(T) specimen, different stress intensity rates are realized by changing the coefficients α and γ in the load versus time function $P(t)$. The evolution histories of biaxiality parameter β with stress intensity factor corresponding to different loading rates for TPB specimens with $a/W = 0.5$ and 0.2 are presented in Figs. 10 and 11, respectively. The effect of loading rate on the biaxiality parameter

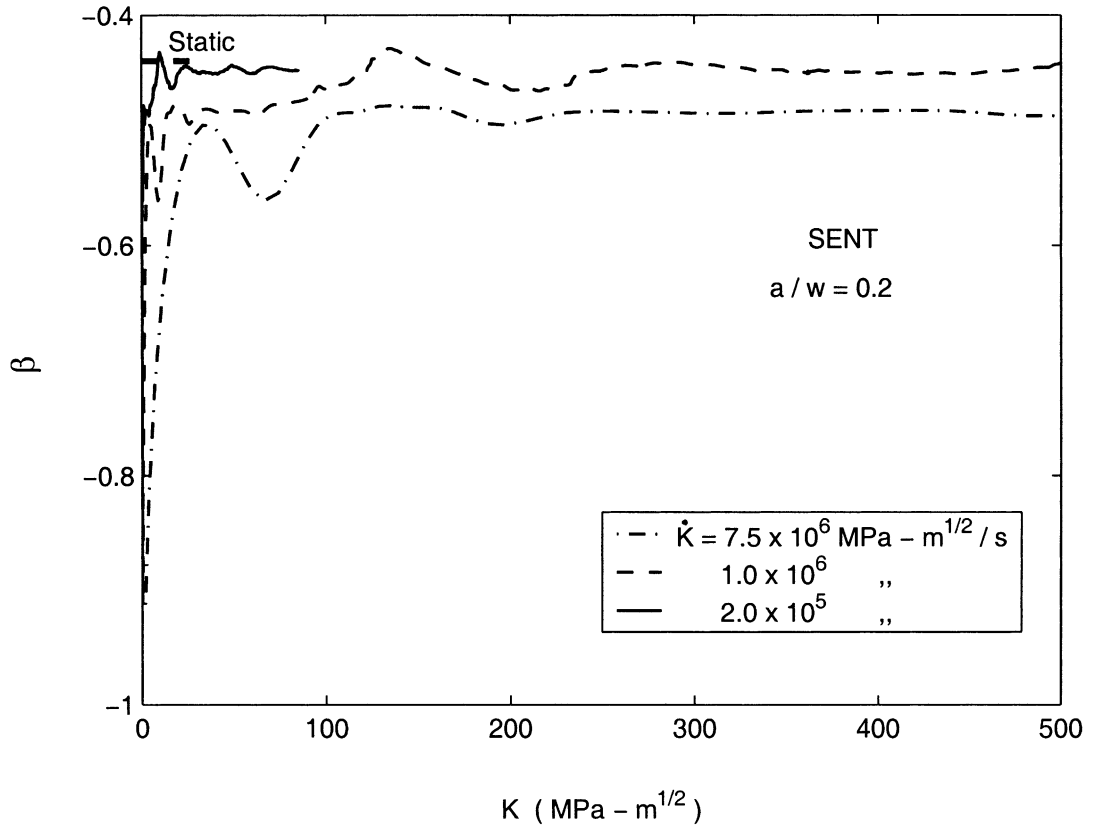

Fig. 8. Evolution histories of biaxiality parameter with stress intensity factor corresponding to different $\dot{K}$ for SEN(T) specimen with $a/W = 0.2$.

for the TPB specimen is qualitatively similar to the SEN(T) specimen. Thus, it may be observed from Figs. 10 and 11 that β has a large negative value during early stages of the loading process if the stress intensity rate is high. At later stages of loading (i.e., at higher values of K), β gradually tends to the static limit. Also, at the same stress intensity rate (see, for example, the curves corresponding to $\dot{K} = 1 \times 10^6$ MPa$\sqrt{\text{m}}$/s in Figs. 10 and 11), β approaches the static limit at lower levels of K for the shallow cracked specimen. The above results indicate that for both the specimen geometries analyzed in this work, inertial effects have a dramatic effect on the biaxiality parameter during early stages of dynamic loading.

3.3. Comparison of evolution histories of β in SEN(T) and TPB specimens

In Fig. 12, the evolution histories of β with stress intensity factor obtained for SEN(T) and TPB specimens with $a/W = 0.5$ corresponding to the same stress intensity rate $\dot{K} = 7.5 \times 10^6$ MPa$\sqrt{\text{m}}$/s are compared. It can be observed from this figure that although β for the above SEN(T) specimen is slightly less than that of the TPB specimen under static loading (see Table 1), the reverse trend applies under highly dynamic loading. Thus, during early stages of dynamic loading (say, $K < 300$ MPa$\sqrt{\text{m}}$), the TPB specimen experiences a much more negative value of biaxiality parameter as compared to the SEN(T) specimen. A

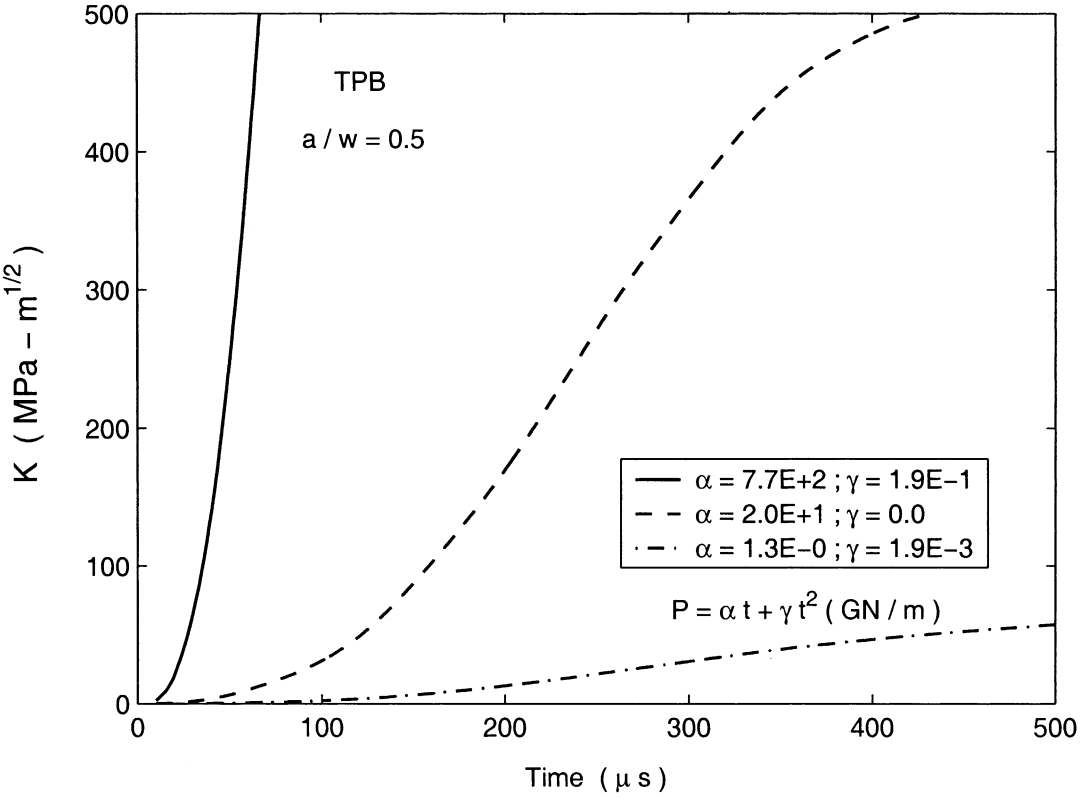

Fig. 9. Typical time histories of stress intensity factor obtained for TPB specimen with $a/W = 0.5$.

similar behaviour was noted by comparing the evolution histories of β for SEN(T) and TPB specimens with other a/W ratios as well. This observation is important since TPB specimens are commonly used in dynamic fracture testing and the large negative β values experienced by these specimens will affect the dynamic fracture toughness data as will be seen in Section 4.

3.4. Variation of stress intensity factor with T-stress

It is instructive to plot the variation of the stress intensity factor with T-stress for different loading rates in order to understand the effect of $\dot{K}$ on the fracture process and, hence, the dynamic fracture toughness (see Section 4). These plots are shown in Fig. 13 for the SEN(T) specimen with $a/W = 0.5$. For comparison, the variation of K with T-stress for this specimen under static loading is also displayed in Fig. 13. This variation is linear since β is constant (independent of K) for a given specimen under static loading. It may be seen from Fig. 13 that the curve pertaining to the low loading rate ($\dot{K} = 2 \times 10^5$ MPa$\sqrt{\text{m}}$/s) is virtually indistinguishable from the linear static variation. The distinction between these two curves may be observed for very low value of K (less than 50 MPa$\sqrt{\text{m}}$) from the inset diagram in Fig. 13 which shows the K versus T variation at initial stages of loading. As $\dot{K}$ increases, it can be seen from Fig. 13 that the K versus T curve shifts to the left of the static line (i.e., T becomes more negative for a given K). It merges with the static line (after oscillating around it) at higher values of K.

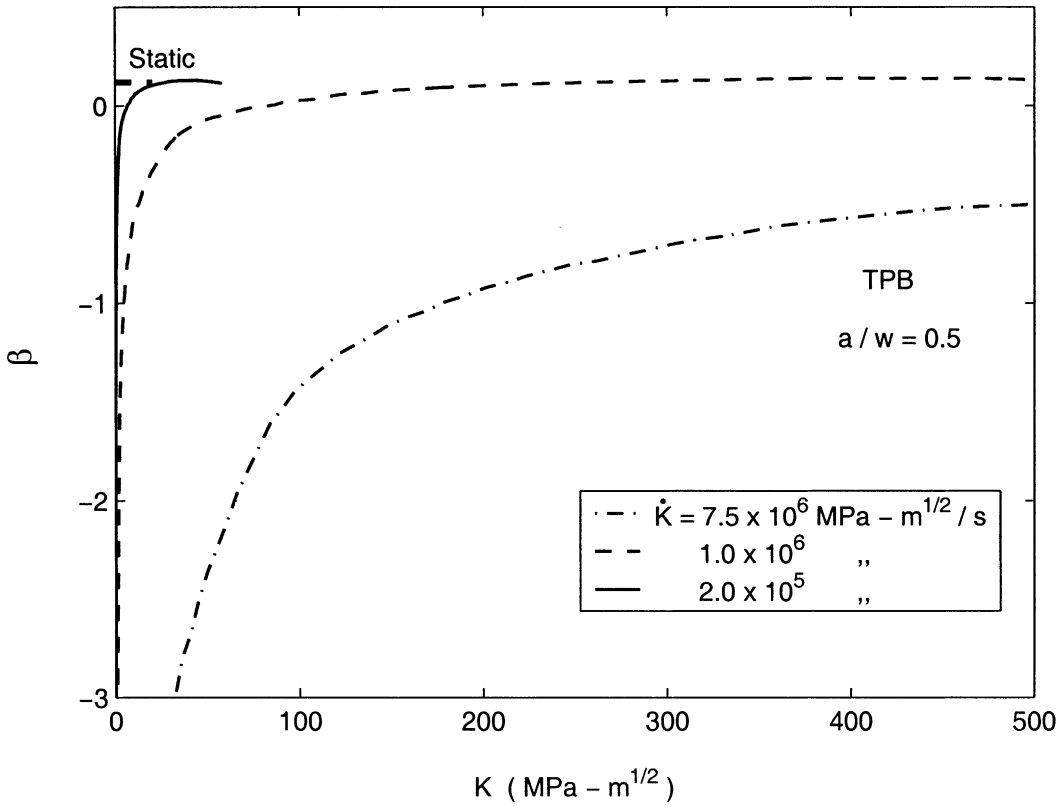

Fig. 10. Evolution histories of biaxiality parameter with stress intensity factor corresponding to different $\dot{K}$ for TPB specimen with $a/W = 0.5$.

4. Dynamic fracture initiation model

In this section, the results obtained in the previous section (in particular, Fig. 13) are combined with the two-parameter (K–T based) fracture characterization suggested by Betegon and Hancock (1991) in order to propose a simple dynamic fracture initiation model. To this end, it is important to recall that studies based on static analyses show that the mode-I fracture toughness of engineering materials increases strongly with negative T-stress. This is true for failure due to ductile void coalescence (Roy and Narasimhan, 1999a,b) as well as due to brittle cleavage (O'Dowd and Shih, 1994; Betegon et al., 1996). Thus, the fracture toughness K_c versus T locus may be represented in the form of the thick curve shown in Fig. 14(a). It is postulated here that this K_c–T locus is characteristic of a material in the sense that it applies equally well for both static and dynamic loading for a given material. This is a reasonable assumption since a negative T-stress would manifest itself in the same way for both static and dynamic loading by retarding the micro-mechanical processes such as void coalescence or cleavage cracking which are operative in the fracture process zone near a crack tip.

The curves depicting the variation of K pertaining to different applied load histories, versus T, for a typical specimen (see, e.g. Fig. 13) are superimposed on the above K_c–T locus in Fig. 14(a). The linear K–T variation pertaining to static loading is also shown in Fig. 14(a) (assuming, for the sake of definiteness, that T is negative under static loading also). As in Fig. 13, the curves corresponding to low $\dot{K}$ (such as dotted

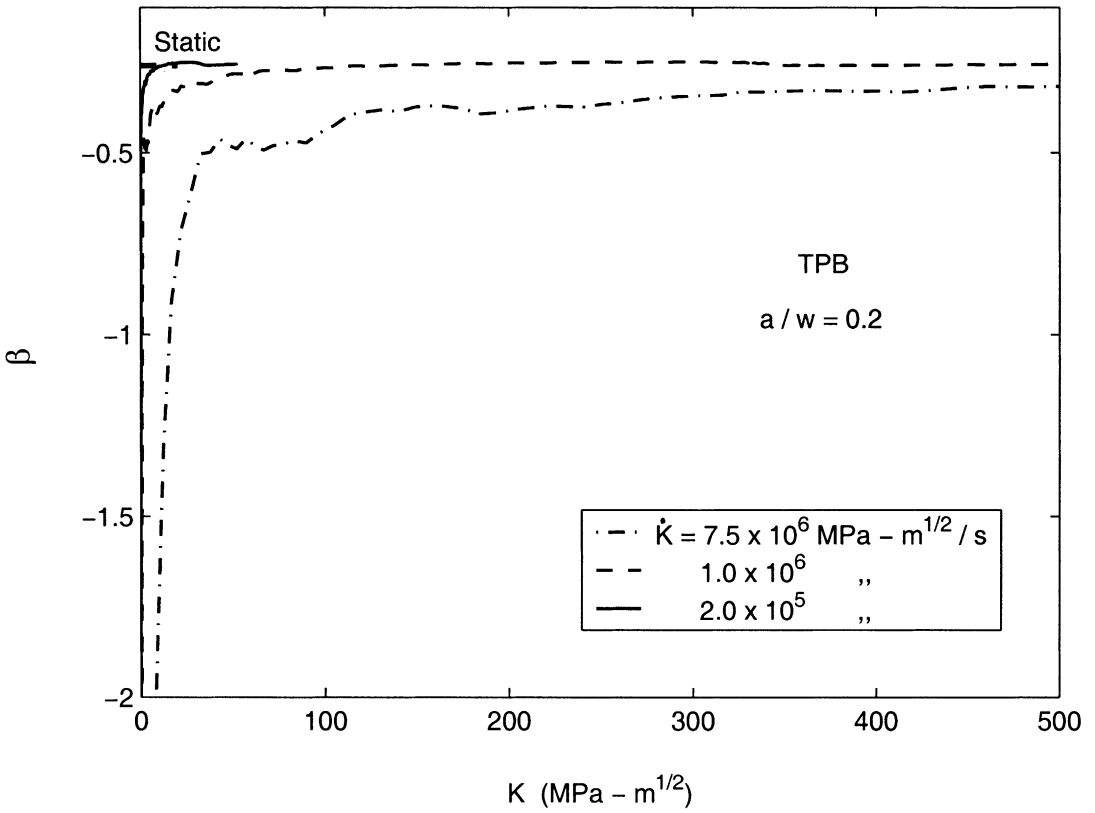

Fig. 11. Evolution histories of biaxiality parameter with stress intensity factor corresponding to different $\dot{K}$ for TPB specimen with $a/W = 0.2$.

curves 1 and 2 in Fig. 14(a)) merge with the static line at small values of K, whereas, those corresponding to higher $\dot{K}$ shift further to the left of the static line. They are expected to merge with the static K–T line at much higher values of K (see also Fig. 13). The point of intersection of the static K–T line with the postulated K_c–T locus will yield the static fracture toughness K_{Ic} that will be obtained from the given specimen (see Fig. 14(a)). Similarly, the point of intersection of each dotted curve with the K_c–T locus will give the value of the dynamic fracture toughness $K_{dc}^{(i)}$ corresponding to a particular loading rate $\dot{K}^{(i)}$. Thus, dotted curves 1 and 2 pertaining to low values of $\dot{K}$ will intersect the K_c–T locus close to K_{Ic}, whereas, the curves pertaining to higher $\dot{K}$ values will intersect the K_c–T locus at higher levels of K.

The variation of K_{dc} with $\dot{K}$, obtained by the above simple model can, now be plotted as shown in Fig. 14(b). This figure shows that K_{dc} will vary negligibly from the static limit K_{Ic} for low loading rates (see points marked as K_{dc}^1 and K_{dc}^2 in Fig. 14(b)). However, at high loading rates, K_{dc} will display a substantial enhancement over the static limit and will also increase steeply with $\dot{K}$. From the curves shown in Fig. 13, the above enhancement is expected to occur for the SEN(T) specimen with $a/W = 0.5$, when $\dot{K}$ exceeds 10^6 MPa $\sqrt{\text{m}}$/s. This agrees qualitatively with the experimental data of dynamic fracture toughness versus $\dot{K}$ obtained recently by Owen et al. (1998a) for 2024-T3 aluminium alloy.

It must be mentioned that the model proposed above assumes that the material response under static and dynamic loading is similar as in the case of rate independent plastic materials. However, for rate dependent plastic solids, the yield stress will be elevated at high loading rates. This enhancement in yield stress is also

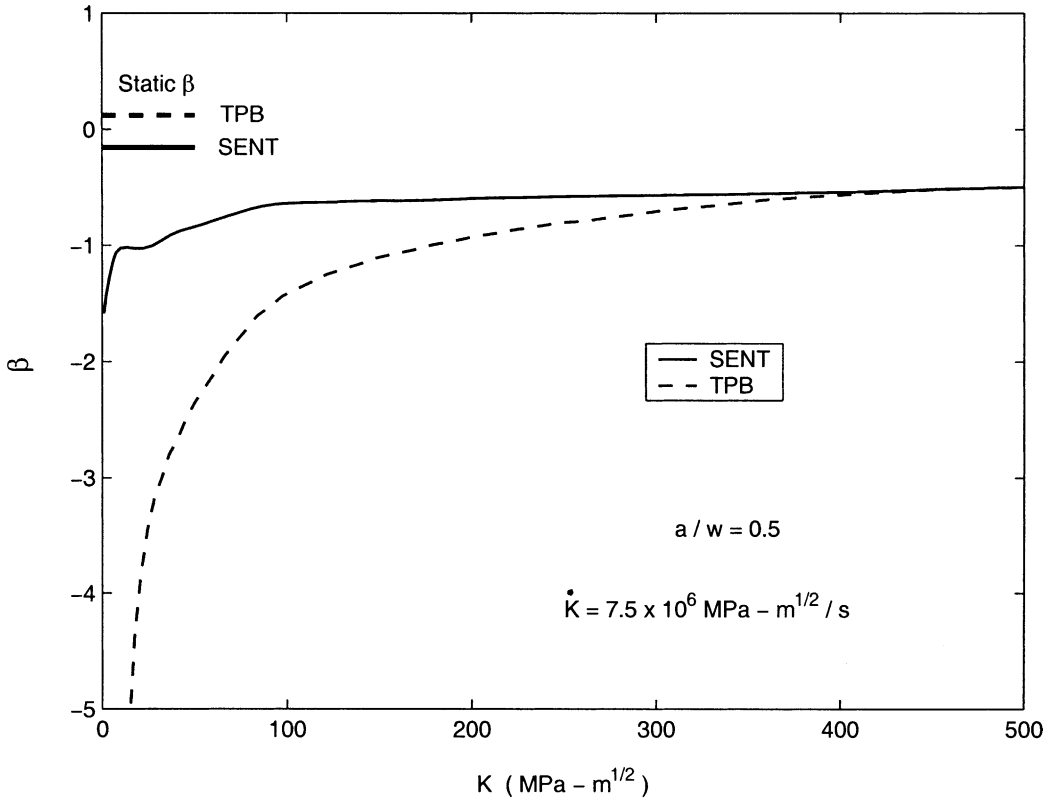

Fig. 12. Comparsion of evolution histories of biaxiality parameter with stress intensity factor for SEN(T) and TPB specimen at the same $\dot{K}$ of 7.5×10^6 MPa $\sqrt{\text{m}}$/s.

expected to affect the variation of dynamic fracture toughness with loading rate. For example, it has been observed by Costin and Duffy (1979) that the cleavage fracture initiation toughness of a rate sensitive steel under dynamic loading is lower than that under static loading. This trend can be rationalized on the basis of the above noted elevation in yield stress at high loading rates (see, also Freund, 1990).

5. Conclusions

In this work, 2-D transient finite element analyses have been carried out to study the effect of loading rate on the T-stress in dynamically loaded single edge notched tension specimens and three point bend specimens. The following are the main conclusions of these analyses.

(1) The biaxiality parameter β under dynamic loading is not a constant for a given specimen geometry like in the static case, but is a function of both the stress intensity factor and the stress intensity rate.

(2) The biaxiality parameter has a large negative value during the early stages of dynamic loading (i.e., for low values of K). This is true for both SEN(T) and TPB specimens, irrespective of crack length, and is very pronounced when $\dot{K}$ is high. However, β approaches the static limit as the magnitude of K increases. The static limit is attained at lower levels of K for shallow cracked specimens as compared to deeply cracked ones for a given $\dot{K}$.

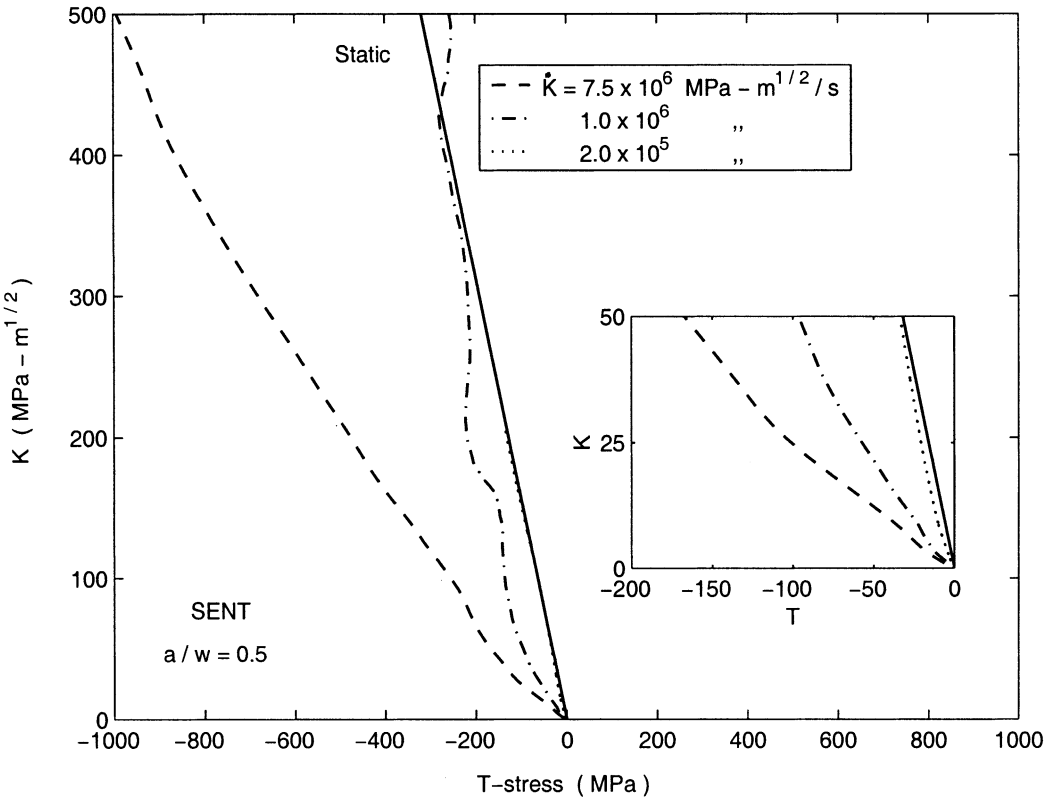

Fig. 13. Variation of stress intensity factor with T-stress for different loading histories (along with the static case) for SEN(T) specimen with $a/W = 0.5$.

(3) The TPB specimen experiences a much more negative value of biaxiality parameter during the early stages of dynamic loading as compared to the SEN(T) specimen with the same normalized crack length a/W when both specimens are subjected to the same stress intensity rate.

(4) A simple model of dynamic crack initiation is proposed which combines a material-specific K_c–T locus along with the K versus T variations for a typical specimen subjected to different loading histories. The model predicts that the dynamic fracture toughness will be close to the static value for low to intermediate stress intensity rates (say, $\dot{K}$ less than 10^6 MPa$\sqrt{\text{m}}$/s), and would show a strong elevation at higher $\dot{K}$ (in excess of 10^6 MPa$\sqrt{\text{m}}$/s). This is in qualitative agreement with experimental results obtained for engineering materials. Thus, the enhancement in fracture toughness at ultra-high loading rates may be attributed to the large negative T-stress experienced by dynamically loaded fracture specimens.

Although the dynamic fracture initiation model proposed in Section 4 qualitatively explains experimentally observed variations of fracture toughness with loading rate, further static and dynamic fracture experiments need to be conducted in order to precisely validate the model. These experiments must be aimed at obtaining the K_c–T locus for typical engineering materials as well as the evolution of stress intensity factor with T-stress for dynamically loaded specimens. These results can then be combined in the manner discussed in Section 4, to obtain the variation of fracture toughness with loading rate, which can be compared with that determined directly from the dynamic fracture experiments.

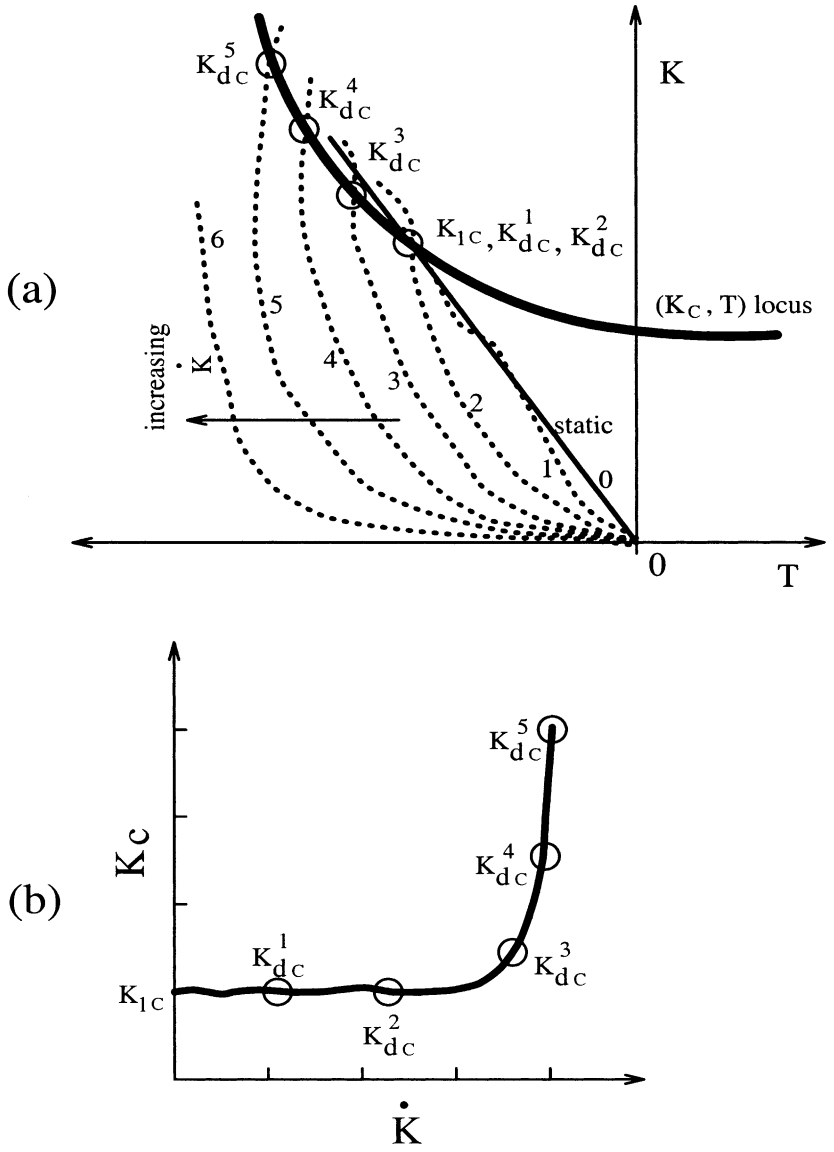

Fig. 14. (a) Schematic showing a material-specific K_c–T locus along with K–T variation corresponding to different loading histories. (b) Dynamic fracture toughness versus $\dot{K}$ predicated by the proposed model.

References

Al-Ani, A.M., Hancock, J.W., 1991. *J*-dominance of short cracks in tension and bending. Journal of the Mechanics and Physics of Solids 39, 23–43.

Basu, S., Narasimhan, R., 1996. Finite element simulation of mode I dynamic, ductile fracture initiation. International Journal of Solids and Structures 33, 1191–1207.

Basu, S., Narasimhan, R., 1999. A finite element study of the effect of material characteristics and crack tip constraint on dynamic ductile fracture initiation. Journal of the Mechanics and Physics of Solids 47, 325–350.

Basu, S., Narasimhan, R., 2000a. A numerical investigation of loss of crack tip constraint in a dynamically loaded ductile specimen. Journal of the Mechanics and Physics of Solids 48, 1967–1985.

Basu, S., Narasimhan, R., 2000b. A comparative study of dynamic, ductile fracture initiation in two specimen configurations. International Journal of Fracture 102, 393–410.

Betegon, C., Hancock, J.W., 1991. Two-parameter characterization of elastic–plastic crack tip fields. Transactions of the ASME Journal of Applied Mechanics 58, 104–110.

Betegon, C., Belzunce, F.J., Rodriguez, C., 1996. A two parameter fracture criterion for high strength low carbon steel. Acta Materialia 44, 1055–1061.

Costin, L.S., Duffy, J., 1979. The effect of loading rate and temperature on the initiation of fracture in a mild, rate-sensitive steel. Transactions of the ASME Journal of Engineering Materials and Technology 101, 258–264.

Dally, J.W., Barker, D.B., 1988. Dynamic measurements of initiation toughness at high loading rates. Experimental Mechanics 28, 298–303.

Freund, L.B., 1990. Dynamic Fracture Mechanics, Cambridge University Press, Cambridge, MA.

Kalthoff, J.F., 1986. Fracture behaviour under high rates of loading. Engineering Fracture Mechanics 23, 289–298.

Kanninen, M.F., O'Donoghue, P.E., 1995. Research challenges arising from current and potential applications of dynamic fracture mechanics to the integrity of engineering structures. International Journal of Solids and Structures 32, 2423–2445.

Kfouri, A.P., 1986. Some evaluations of the elastic T-term using Eshelby's method. International Journal of Fracture 30, 301–315.

Kirk, M.T., Koppenhoefer, K.C., Shih, C.F., 1993. Effect of constraint on specimen dimensions needed to obtain structurally relevant toughness measures. ASTM STP 1171, 79–103.

Koppenhoefer, K.C., Dodds, R.H., 1996. Constraint effects on fracture toughness of impact-loaded, precracked Charpy specimens. Nuclear Engineering and Design 162, 145–158.

Larsson, S.G., Carlsson, A.J., 1973. Influence of non-singular stress terms and specimen geometry on small-scale yielding at crack tips in elastic–plastic materials. Journal of the Mechanics and Physics of Solids 21, 263–278.

Liu, C., Knauss, W.G., Rosakis, A.J., 1998. Loading rates and the dynamic initiation toughness in brittle solids. International Journal of Fracture 90, 103–118.

Nakamura, T., Shih, C.F., Freund, L.B., 1986. Analysis of a dynamically loaded three-point bend ductile fracture specimen. Engineering Fracture Mechanics 25, 333–339.

O'Dowd, N.P., Shih, C.F., 1992. Family of crack-tip fields characterized by a triaxiality parameter - II. Fracture applications. Journal of the Mechanics and Physics of Solids 40, 939–963.

O'Dowd, N.P., Shih, C.F., 1994. Two-parameter fracture mechanics: Theory and applications. ASTM STP 1207, 21–47.

Owen, D.M., Zhuang, S., Rosakis, A.J., Ravichandran, G., 1998a. Experimental determination of dynamic crack initiation and propagation fracture toughness in thin aluminum sheets. International Journal of Fracture 90, 153–174.

Owen, D.M., Rosakis, A.J., Johnson, W.L., 1998b. Dynamic failure mechanisms in beryllium-bearing bulk metallic glasses. SM Report 98-22, GALCIT, California Institute of Technology, Pasadena, USA.

Ravi-Chandar, K., Knauss, W.G., 1984. An experimental investigation into dynamic fracture: I. Crack initiation and arrest. International Journal of Fracture 25, 247–262.

Roy, A.Y., Narasimhan, R., Arora, P.R., 1999. An experimental investigation of constraint effects on mixed mode fracture initiation in a ductile aluminium alloy. Acta Materialia 47, 1587–1596.

Roy, A.Y., Narasimhan, R., 1999a. Constraint effects on ductile fracture processes near a notch tip under mixed-mode loading. Engineering Fracture Mechanics 62, 511–534.

Roy, A.Y., Narasimhan, R., 1999b. A finite element investigation of the effect of crack tip constraint on hole growth under mode I and mixed mode loading. International Journal of Solids and Structures 36, 1427–1447.

Sladek, J., Sladek, V., Fedelinski, P., 1997. Integral formulation for elastodynamic T-stresses. International Journal of Fracture 84, 103–116.

Sumpter, J.D.G., Forbes, A.T., 1992. Constraint based analysis of shallow cracks in mild steel. Proceedings of TWI/EWI/IS International Conference on Shallow Crack Fracture Mechanics Test and Applications, Cambridge, UK.

Venkert, A., Guduru, P.R., Ravichandran, G., 1998. Mechanisms of dynamic failure in Ni–Cr steels. SM Report 98-5, GALCIT, California Institute of Technology, Pasadena, USA.

Williams, M.L., 1957. On the stress distribution at the base of a stationary crack. Transactions of ASME Journal of Applied Mechanics 24, 109–114.

Zehnder, A.T., Rosakis, A.J., 1990. Dynamic fracture initiation and propagation in 4340 steel under impact loading. International Journal of Fracture 43, 271–285.

Zehnder, A.T., Rosakis, A.J., Krishnaswamy, S., 1990. Dynamic measurement of the J integral in ductile metals: Comparison of experimental and numerical techniques. International Journal of Fracture 42, 209–230.

Zienkiewicz, O.C., Taylor, R.L., 1989. The finite element method, Solid and Fluid Mechanics Dynamics and Non-linearity, fourth ed., vol. 2. McGraw-Hill, UK.